Reconciliation of Experiments and Theory on Transport Properties of Iron and the Geodynamo

Youjun Zhang,[1,2,*] Mingqiang Hou,[2,3,*] Guangtao Liu,[2] Chengwei Zhang,[2] Vitali B. Prakapenka,[4] Eran Greenberg,[4] Yingwei Fei,[5] R. E. Cohen,[5,†] and Jung-Fu Lin[6,‡]

[1]*Institute of Atomic and Molecular Physics, Sichuan University, Chengdu 610065, China*
[2]*Center for High Pressure Science and Technology Advanced Research (HPSTAR), Shanghai 201900, China*
[3]*The Advanced Light Source, Lawrence Berkeley National Laboratory, Berkeley, California 94720, USA*
[4]*Center for Advanced Radiation Sources, University of Chicago, Chicago, Illinois 60637, USA*
[5]*Extreme Materials Initiative, Earth and Planets Laboratory, Carnegie Institution for Science, Washington, DC 20015-1305, USA*
[6]*Department of Geological Sciences, Jackson School of Geosciences, The University of Texas at Austin, Austin, Texas 78712, USA*

(Received 6 January 2020; accepted 13 July 2020; published 13 August 2020)

We measure the electrical resistivity of hcp iron up to ~170 GPa and ~3000 K using a four-probe van der Pauw method coupled with homogeneous flattop laser heating in a DAC, and compute its electrical and thermal conductivity by first-principles molecular dynamics including electron-phonon and electron-electron scattering. We find that the measured resistivity of hcp iron increases almost linearly with temperature, and is consistent with our computations. The results constrain the resistivity and thermal conductivity of hcp iron to $\sim 80 \pm 5\ \mu\Omega\,\mathrm{cm}$ and $\sim 100 \pm 10\ \mathrm{W\,m^{-1}\,K^{-1}}$, respectively, at conditions near the core-mantle boundary. Our results indicate an adiabatic heat flow of $\sim 10 \pm 1$ TW out of the core, supporting a present-day geodynamo driven by thermal and compositional convection.

DOI: 10.1103/PhysRevLett.125.078501

Earth's core works like a heat engine through heat transfer from the cooling and freezing of the liquid iron core, which powers the present-day geodynamo, mantle convection, and plate tectonics [1,2]. Paleomagnetic records indicate that the geodynamo has been active for at least 3.4 Gyr [3]. The geodynamo was long believed to be driven by primordial heat in the Earth being transported by thermal convection through the liquid outer core, which depends on the transport properties of iron at extreme conditions [4,5]. Heat flow of 3–4 TW across the core-mantle boundary (CMB) may suffice to sustain the geodynamo from the early history of Earth's core, indicating an old inner core of ~3.5 Gyr [6]. However, first-principles calculations by Refs. [7] and [8] claimed a much higher adiabatic heat flow (15–20 TW) at the CMB, and estimated thermal conductivity κ of $150\ \mathrm{W\,m^{-1}\,K^{-1}}$ in pure Fe [7,8]. Their conductivity value is three to five times higher than geophysical estimates and shock experiments [6,9–11]. This discrepancy ignited a debate on the geodynamo, Earth's energy budget, and thermal evolution of the core. Present scenarios include convection driven by chemical differentiation rather than thermal convection [12], which requires a different process for each planetary dynamo, as opposed to thermal convection, which acted as a universal concept for driving planetary dynamos. Nevertheless, thermal evolution models show that even these higher conductivities can be consistent with a thermally driven dynamo when radiogenic heating of the core is included [13]. The conductivity values of iron in the core also influence our assessment of the age of the inner core formation: the higher the electrical and thermal conductivities are, the faster Earth's core cools, and the younger the inner core [1].

Several experimental studies have been conducted at high *P-T* conditions, but measurements of the transport properties of Fe using different methods came to dramatically contradictory results [5,14–17]. The current estimate of thermal conductivity of iron under CMB conditions varies by a factor of ~6 in laser-heated DAC experiments (summarized in Table S1 [18], which includes Refs. [5–9,14,15,19–27]); this translates into the CMB heat flux of 4–20 TW. A very high thermal conductivity of $226^{+71}_{-31}\ \mathrm{W\,m^{-1}\,K^{-1}}$ in hcp Fe at the topmost outer core was derived via the Wiedemann-Franz law ($\kappa = LT/\rho$) through electrical resistivity (ρ) measurements [14,17]. However, direct thermal conductivity measurements of hcp Fe gave a low thermal conductivity o f $33 \pm 7\ \mathrm{Wm^{-1}\,K^{-1}}$ near the CMB [15,28,29]. New theoretical calculations show that both electron-phonon and electron-electron scatterings contribute to the thermal conductivity of iron, and give a value of $97 \pm 10\ \mathrm{W\,m^{-1}\,K^{-1}}$ for hcp Fe at the CMB conditions, and modify the Wiedemann-Franz law [20]. Electron correlations beyond density functional theory (DFT) increase the resistivity by about 35% at Earth's core conditions over the conventional DFT values, and reduce the thermal conductivity by a similar factor [20]. The computed thermal conductivity is between those inferred from the experimental thermal conductivity and electrical resistivity measurements.

The discrepancy [30,31] between the thermal conductivity and resistivity measurements may arise from temperature gradients in the laser-heated samples, sample deformation and textures, probe geometry, and the breakdown of ideal Wiedemann-Franz law (see Supplemental Material [18], which includes Refs. [7,8,14,17,20,32–34]). Uncertain thermal conductivity of the core may result in a big difference in our understanding of the thermal history of the core and its geodynamo [35,36]. Thus, further improved and integrated experimental measurements and theoretical studies on the transport properties of Fe at high *P-T* are needed.

We used a modified four-probe van der Pauw method [37] to reliably measure the electrical resistivity of hcp Fe at high *P-T* in a double-side laser-heated DAC with two flattop laser beams [38] (see Supplemental Material [18,39]). An iron sample (~2 μm thick) was shaped into a uniform Greek cross sheet with a circular region of ~6 μm at the central cross area (cloverleaf) using a focused ion beam (FIB) [Fig. 1(a)]. The cross sheet has four arms with a length of ~70 μm, which act as internal electrode wires [Fig. 1(b)]. The arms were connected to four external Pt leads. The heart area of the cloverleaf matches well with a finely focused laser-heating spot [~10 μm, Fig. 1(c)]. Our samples have a smaller width than the laser spot, ensuring homogeneous flattop heating with uniform temperature distributions on both sides of the sample. The Greek cross sheet with a diameter varied from ~6 μm to hundreds of micrometers has been proved to be a valid van der Pauw test structure by theory and experiment [37,40]. The sample assembly also avoids contact resistance and contamination from possible alloying between Pt leads and Fe sample.

We first measured the electrical resistivity of hcp Fe up to ~140 GPa at room temperature. The pressures and volumes were determined by the thermal equation of state [41] of hcp Fe from *in situ* synchrotron x-ray diffraction at high *P-T* (example patterns in Fig. S1 in the Supplemental Material [18]) during the resistivity measurements at GSECARS, Advanced Photon Source. The resistivity in hcp Fe decreases with increasing pressure (Fig. S2 [18]), consistent with previous studies [5,16]. We then measured resistivity at ~105 GPa with increasing temperature up to ~3000 K (Fig. 2); the resistivity increases with increasing temperature almost linearly, with an intercept of ~4.8 $\mu\Omega$ cm at room temperature. The temperature dependence of our data is very different from the result of previous experiments [14], which showed a significant reduction of resistivity with temperature (Fig. 2). Our measured resistivity is around 1.6 times higher than Ref. [14] up to 3000 K at ~105 GPa. This difference is likely due to the temperature gradient and sample geometry in the earlier experiments. We tested this at ~74 GPa by introducing an artificial temperature gradient, in which we heated one corner of a relatively large sample of ~15 μm in diameter compared to the focused laser spot of ~10 μm (Fig. S3a in the Supplemental Material [18]). When the laser spot size and position did not match well with the sample, we observed strong resistivity saturation similar to what was reported in Ref. [14] (Fig. S3b in the Supplemental Material [18]). The details on the temperature gradient issue are discussed in the Supplemental Material [18].

We carried out additional high-temperature experiments using homogeneous laser-heated DACs up to ~3000 K from ~82 to ~165 GPa, where only hcp Fe was observed (Fig. S4 [18]). We analyzed the temperature distribution on a sample with ~6 μm width at ~2 380 K and ~142 GPa. It shows a very homogeneous temperature in a width of ~8 μm (Fig. S5 in the Supplemental Material [18]), which matched well with the sample size. The measured resistivities at 82, 133, 142, and 165 GPa are shown in Figs. S6a–S6d in the Supplemental Material [18], respectively. We found that the resistivity for all these well-heated Fe samples in our experiments increased quasilinearly with increasing temperatures up to ~3000 K in experiments. The results could be fitted well with the Bloch-Grüneisen formula at the measured *P-T* range (solid blue curves, Fig. 2) (see Supplemental Material and Table S2 [18,42]).

We compare our experimental data with computations of transport properties that include *e*-ph and *e*-*e* scattering based on first-principles lattice dynamics and density functional perturbation theory (DFPT) [20], and also with our new results using first-principles molecular dynamics (FPMD) (see Supplemental Material and Fig. S7 [18],

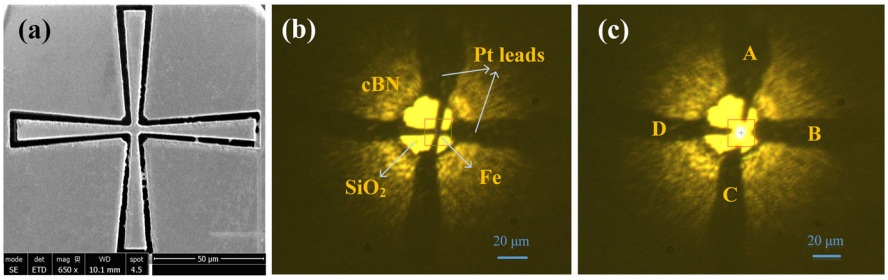

FIG. 1. Photograph of a shaped iron foil and the sample loaded in a laser-heated diamond anvil cell (DAC). (a) A Greek cross sheet of iron shaped by FIB; and (b) a loaded sample in a DAC with a culet of 300 μm beveled to 75 μm at ~142 GPa and 300 K and then laser heated to 2400 K (c). Pt leads had a width of ~20 μm and a thickness of ~4 μm. The laser was focused into a flattop shape on the circular section of the Fe sample with ~6 μm in diameter.

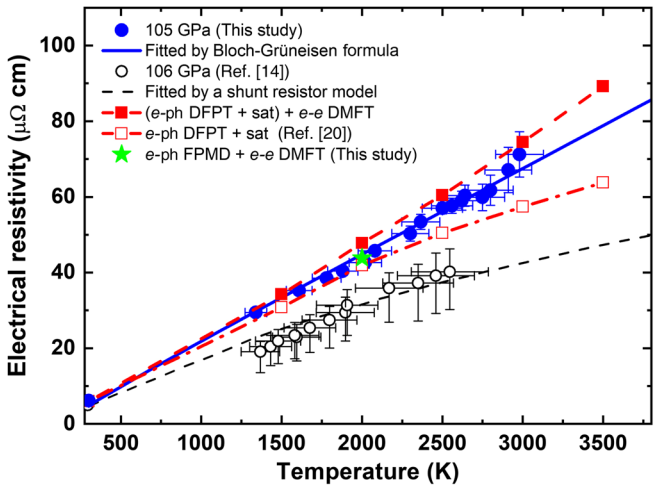

FIG. 2. Measured and calculated resistivity of hcp Fe at ~105 GPa with increasing temperature up to ~2980 K in a laser-heated DAC. The pressure of 105 GPa was determined at ambient temperature by x-ray diffraction. At ~2980 K, the pressure is about 117 GPa according to the thermal equation of state of hcp Fe [41]. Our measurements are compared with the current calculations that considered both *e*-ph and *e*-*e* contributions by DFPT + DMFT (Ref. [20], solid squares) and new calculations by FPMD + DMFT (this study, solid green star), and also compared with previously measured resistivity [14] (open circles) and calculations considered only *e*-ph contribution (Ref. [20], open red squares). *e*-ph is the electron-phonon contribution of resistivity calculated by DFPT with inelastic Boltzmann theory, *e*-*e* is the electron-electron contribution of resistivity, and "sat" is resistivity saturation effects for the *e*-ph scattering. The red dashed line through the calculated resistivity is a guide to the eye. The solid blue curve is fitted using the Bloch-Grüneisen formula for the measured resistivity. The black short dashed line represents the saturated resistivity fitted by a shunt resistor model in Ref. [14].

which includes Refs. [43,44]). In the former computations, the *e*-ph contribution was computed using the inelastic Boltzmann transport equation [45] and DFPT; and the *e*-*e* contribution was obtained using density functional theory and dynamical mean field theory (DFT + DMFT) [46,47]. Now we have performed further FPMD computations, and evaluated transport properties using DFT + DMFT. Any saturation effects are included automatically and naturally in the FPMD (see Fig. S7 and discussion in Supplemental Material [18], which includes Refs. [48–54]). Neither the present calculations, nor those in Ref. [20] use fitting to data to obtain saturation effects, but the previous work relied on a model of saturation based on mean-free path and assumed Matthiessen's rule, that *e*-*e* and *e*-ph scattering can be computed separately and added. Our new measurements are consistent with the computed resistivities by DFPT and DMFT (Ref. [20]) (solid red squares and dashed red line in Fig. 2). In addition, the calculation is also consistent with a model that assumes a Bloch-Grüneisen form fit to our data (Fig. 2). Using separately computed *e*-ph and *e*-*e* scattering with a model for saturation effects in Ref. [20] gives about 10% higher resistivity than that extrapolated from the Bloch-Grüneisen formula up to 3500 K. Using FPMD with DFT and DMFT we obtain new results that agree perfectly with our new experimental results for hcp Fe in Fig. 2 (solid green star). It is encouraging that a very different theoretical technique based on FPMD and very different assumptions agrees well with first-principles lattice dynamics results that include a model for resistivity saturation. The measured resistivity of hcp Fe is also compared with the calculated resistivity contributed only by *e*-ph scattering (Ref. [20], open red squares and dash-dotted red line in Fig. 2). One can see that the *e*-*e* contribution to the resistivity is less than 10% at ~1500 K, but it reaches above ~20% to 3000 K at ~105 GPa, indicating a non-negligible effect of *e*-*e* scattering on the resistivity of hcp Fe by both the experiments and theories, especially at high temperatures. The effects on thermal conductivity are larger, as discussed in Ref. [20], indicating a nonideal Lorenz number at high *P*-*T*.

To estimate transport properties for Earth's core, we extrapolated the resistivity of hcp Fe up to 4000 K above 133 GPa by the Bloch-Grüneisen formula [Fig. 3(a) and Fig. S6 [18]]. The electrical resistivity is found to be $\sim 80 \pm 5\ \mu\Omega\,\mathrm{cm}$ in hcp Fe near CMB conditions (~136 GPa and 4000 K). Compared with the previous data by DAC experiments (Ref. [14]), our results show about 1.5 to 2 times higher resistivity at the relevant conditions of the outer core [Fig. 3(a)]. Our determined resistivity of hcp Fe at ~140 GPa and ~3000 K generally agree with the previous shock experiment by Ref. [11] but significantly smaller than the one by Ref. [10] [Fig. 3(a)]. Future shock experiments are needed to find out the reason for the large difference in these studies. Based on the computed resistivity and thermal conductivity of hcp Fe at the CMB conditions (Ref. [20]), the Lorenz number is estimated to be $\sim(2.0\text{–}2.1) \times 10^{-8}\ \mathrm{W\Omega\,K^{-2}}$, which is ~20% lower than the ideal value (Supplemental Material and Fig. S8 [18], which includes Refs. [55–57]). Comparing the Lorenz number with that obtained by Ref. [7] [open diamonds in Fig. 3(b)] shows that our finding is ~10% lower than that calculated from molecular dynamics simulation without *e*-*e* scattering for Fe. We convert the experimental resistivity data for hcp Fe at high *P*-*T* to the thermal conductivity using the computed Lorenz number in the Wiedemann-Franz law, and obtain a thermal conductivity significantly lower than the previous estimates by Ref. [14] that used the ideal Lorenz number ($2.44 \times 10^{-8}\ \mathrm{W\Omega\,K^{-2}}$) [Fig. 3(b)]. At about 136 GPa and 4000 K, at near CMB conditions, we find that the thermal conductivity in hcp Fe is around $100 \pm 10\ \mathrm{W\,m^{-1}\,K^{-1}}$. Our values are still somewhat higher than the results measured by Ref. [15] through direct observations of heat pulse in hot dense hcp Fe, and deviate more with their extrapolated values with increasing pressure. Thus, it seems that the previous electrical conductivity was too high, and the previous thermal conductivity was too low.

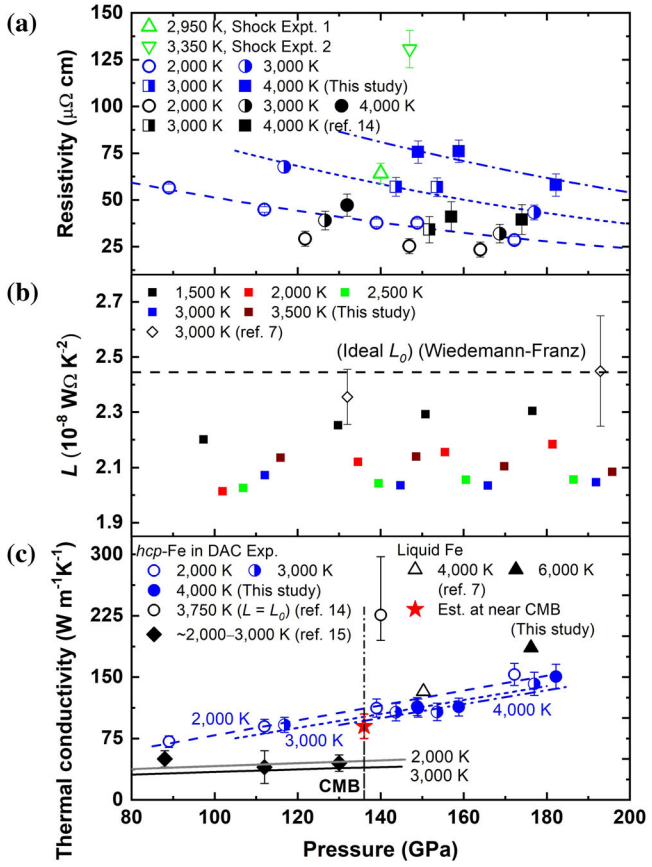

FIG. 3. Electrical resistivity and thermal conductivity of Fe at the relevant P-T conditions of Earth's core. (a) Our experimental results of hcp Fe at 2000 K (open blue circles) and 3000 K (semiopen blue circles), respectively, and the extrapolated data by Bloch-Grüneisen formula at 3000 K (semiopen blue squares) and 4000 K (solid blue squares), respectively. Our measured resistivities are compared with previous results (Ref. [14]) at 2000 K (open black circles), 3000 K (semiopen black circles), and 4000 K (solid black circles) in laser-heated DACs, respectively, and their extrapolated data by a resistivity saturation model at 3000 K (semiopen black squares) and 4000 K (solid black squares), respectively, and also compared with shock experiments (green open triangle [11] and inverted triangle [10]). (b) Calculated Lorenz number (L) as functions of pressure and temperature. The ideal Lorenz number $L_0 = 2.44 \times 10^{-8}$ WΩ K^{-2}. The calculated Lorenz number in liquid Fe (Ref. [7]) is also plotted for comparison (open diamonds). (c) The thermal conductivity of hcp Fe and liquid Fe derived using the Wiedemann-Franz relation at the relevant conditions of the outer core. The thermal conductivities are compared with previous results derived from resistivity experiments (open black circle, Ref. [14]) and from monitoring a heat pulse propagation (solid black diamonds, Ref. [15]), respectively. The star represents the derived thermal conductivity of liquid Fe in this work at near CMB conditions (~136 GPa and ~4000 K), which is compared with the calculated DFT results for liquid Fe at 4000 K (open black triangle) and 6000 K (solid black triangle) [7], respectively. The lines through the experimental points are guides to the eye, where dashed, short-dashed, and dash-dotted lines represent the electrical resistivity and thermal conductivity as a function of pressure at 2000, 3000, and 4000 K, respectively. The vertical dash-dotted line represents the CMB.

Our theory and experiment results fall between the above two previous studies [14,15]. The effect of hcp Fe texture in a DAC on the electrical anisotropy is estimated to be approximately 10%, whereas recent calculations show the electrical anisotropy between c and a axis to be ~26% at Earth's core P-T conditions [20]. A recent study reported approximately 30% anisotropy in modeled thermal conductivity of textured hcp Fe samples at 20–45 GPa and 300 K [58], which are generally consistent with the first-principles estimates (Ref. [20]). A very large anisotropy of $k_c/k_a = 3$-4 for hcp Fe at relevant core P-T conditions was suggested by an extrapolation of the limited data to Earth's core, but the uncertainty is too large to be credible for our understanding of the core geodynamo [58]. Therefore, the discrepancy between this study and previous experimental values cannot be simply explained by textures of hcp Fe crystals (see Supplemental Material [18], which includes Refs. [59–62]).

The outer core is liquid so the effects of melting on the thermal conductivity should be considered. Previous high P-T experiments in heated multianvil apparatuses show a ~5%–10% resistivity increase upon melting from fcc Fe below ~10 GPa [25,26,63,64]. It is still difficult to directly measure the resistivity of liquid Fe in experiments at core conditions so that we have to estimate the effects of the melting of hcp Fe. The recently computed resistivity and thermal conductivity considered the scattering of electrons from both atomic motions (e-ph) and electrons (e-e) shows a 7%–10% increase in resistivity or decrease in thermal conductivity upon melting from hcp structure at 4000–5000 K and ~145 GPa (Ref. [20]), which is slightly lower than previous calculations of ~15% change, which only considered e-ph contributions (Ref. [24]). Therefore, if we use a value of ~10% increase of resistivity after melting, the thermal conductivity of liquid Fe would be around 90 ± 15 W m^{-1} K^{-1} at the relevant condition of the CMB [solid red star, Fig. 3(b)].

Earth's outer core contains ~8 wt % light elements, such as Si, O, S, and C [65], and about 5 wt % Ni. Si, S, and O are proposed to be the most likely major light element(s) based on recent studies [66,67]. Each weight percent of Si, S, and O light elements could reduce the thermal conductivity by 2%–4% near CMB conditions in recent calculations and high-pressure experiments [7,16,27,68]. Thus, an additional 20%–30% decrease in the thermal conductivity is reasonable by the light element impurities of 8–10 wt % for an Fe-Si-O/Fe-S-O outer core. Consequently, the thermal conductivity for liquid Fe alloy at the CMB conditions (κ_{CMB}) would be 70 ± 10 W m^{-1} K^{-1}, which is 30%–50% smaller than previous DFT computations (~100–140 W m^{-1} K^{-1}) [7,8]. We should note that future collaborative experimental and theoretical studies with smaller uncertainties on melting and alloying effects of Ni and light elements on the thermal conductivity of iron at realistic outer core P-T conditions are needed to more accurately interrogate the heat flux paradox.

With taking a CMB temperature of ~3 900 ± 200 K and using results of recent studies on a Si-rich Fe alloy [69], the isentropic heat conduction down the outer core adiabat would be further constrained to be ~10 ± 1 TW (Supplemental Material [18,70,71]), which contributes ~22% in Earth's global interior heat loss (46 ± 3 TW) [2]. The adiabatic heat flow of ~10 ± 1 TW near the topmost outer core in this study is comparable to the recent heat flow estimates (7–13 TW) from the lowermost mantle, which was estimated from the reported lattice thermal conductivity of silicates and oxides (~8–15 $W m^{-1} K^{-1}$) at the lowermost mantle conditions (Table S1 [18], which includes Refs. [2,10,72–79]). According to a recent model of heat budget in the core [13], our estimated CMB thermal heat flux of ~10 TW can be mainly contributed from a secular cooling associated with the heat capacity of the core (~4.8 TW), the latent heat associated with the freezing of the inner core (~3.3 TW), and the gravitational energy associated with the light element partitioning across the inner-core boundary (~2.0 TW) (Fig. S11 and Supplemental Material [18,80,81]). Both thermal and compositional convections play an equally important role in driving the present-day geodynamo. In addition, our determined thermal conductivity at the topmost core (~70 $W m^{-1} K^{-1}$) supports a geodynamo driven by thermal convection over Earth's history [36] and therefore solved the "core paradox" raised by Olson [82].

Based on the recent modeling of the core thermal evolution [4,5] and the thermal heat flux of 10 TW across the CMB, the age of the inner core is constrained to be 1.0–1.3 Gyr. This is significantly lower than some estimates of 3.5–4.2 Gyr [6,15], but higher than recent claims of less than ~0.7 Gyr [14]. Our study points to a 30%–50% reduction in the thermal conductivity of iron alloy as compared with previous studies (~100–140 $W m^{-1} K^{-1}$) at near CMB conditions [5,7,8,14], which could translate into a difference in the estimated inner-core age as large as a factor of 2. We should note that the estimation of the inner core age also depends on the thermal conductivity of the lowermost mantle materials and radioactivity in the core [13]. An increase in both average field strength and variability of Earth's palaeomagnetic field was observed to occur between 1.0 to 1.5 Gyr [83]. Our results would provide an explanation for the change of the observed palaeomagnetic field by the nucleation of Earth's inner core. However, recent magnetic evidence from samples of the ~0.565 Gyr Sept-Îles intrusive suite shows an anomalous palaeomagnetic field during the Ediacaran period [84], indicating a young inner core of 0.5–0.7 Gyr. Therefore, further interrogations between mineral physics, geodynamics, and paleomagnetism are needed to resolve this discrepancy.

We thank Junqing Xu, Kai Luo, Peng Zhang, P. Driscoll, T. Becker, and Jin Liu for helpful discussions. We thank N. P. Salke, J. C. Liu, Y. G. Wang, Q. Zhang, and H. Yang for their assistance with experiments. We acknowledge Y. P. Yang and Z. L. Fan for the FIB cutting. We thank X. Y. Du for the analyses of the temperature distribution. We appreciate Wenge Yang and Rossi Paul for the use of electrical resistivity measurement system. This work was supported by the National Natural Science Foundation of China (41804082) and the National Science Foundation (NSF) with Grants No. EAR-1901813 and No. EAR-1901801. Y. Z. acknowledges the Fundamental Research Funds for the central universities in China. We acknowledge High Pressure Synergetic Consortium (HPsynC), Carnegie Institution for Science for the use of the Keithley ultralow voltage (2182A model) and current source (6221 model) in the resistivity experiments. Portions of this work (*in situ* x-ray diffraction measurements and laser heating) were performed at GeoSoilEnviroCARS (GSECARS), Advanced Photon Source (APS), Argonne National Laboratory. GSECARS is supported by the National Science Foundation-Earth Sciences (EAR-1634415) and Department of Energy-GeoSciences (DE-FG02-94ER14466). This research used resources of the Advanced Photon Source, a U.S. Department of Energy (DOE) Office of Science User Facility operated for the DOE Office of Science by Argonne National Laboratory under Contract No. DE-AC02-06CH11357. R. E. C. was supported by the Carnegie Institution for Science and gratefully acknowledges the Gauss Centre for Supercomputing e.V. for funding this project by providing computing time on the GCS Supercomputer Supermuc-NG at Leibniz Supercomputing Centre.

*These authors contributed equally to this work.
†rcohen@carnegiescience.edu
‡afu@jsg.utexas.edu

[1] C. Davies, M. Pozzo, D. Gubbins, and D. Alfe, Nat. Geosci. **8**, 678 (2015).
[2] T. Lay, J. Hernlund, and B. A. Buffett, Nat. Geosci. **1**, 25 (2008).
[3] J. A. Tarduno, R. D. Cottrell, M. K. Watkeys, A. Hofmann, P. V. Doubrovine, E. E. Mamajek, D. Liu, D. G. Sibeck, L. P. Neukirch, and Y. Usui, Science **327**, 1238 (2010).
[4] S. Labrosse, Phys. Earth Planet. Inter. **247**, 36 (2015).
[5] H. Gomi, K. Ohta, K. Hirose, S. Labrosse, R. Caracas, M. J. Verstraete, and J. W. Hernlund, Phys. Earth Planet. Inter. **224**, 88 (2013).
[6] F. D. Stacey and D. E. Loper, Phys. Earth Planet. Inter. **161**, 13 (2007).
[7] N. de Koker, G. Steinle-Neumann, and V. Vlček, Proc. Natl. Acad. Sci. U.S.A. **109**, 4070 (2012).
[8] M. Pozzo, C. Davies, D. Gubbins, and D. Alfè, Nature (London) **485**, 355 (2012).
[9] F. D. Stacey and O. L. Anderson, Phys. Earth Planet. Inter. **124**, 153 (2001).
[10] Y. Bi, H. Tan, and F. Jing, J. Phys. Condens. Matter **14**, 10849 (2002).

[11] R. N. Keeler and A. C. Mitchell, Solid State Commun. **7**, 271 (1969).
[12] J. G. O'Rourke and D. J. Stevenson, Nature (London) **529**, 387 (2016).
[13] P. Driscoll and D. Bercovici, Phys. Earth Planet. Inter. **236**, 36 (2014).
[14] K. Ohta, Y. Kuwayama, K. Hirose, K. Shimizu, and Y. Ohishi, Nature (London) **534**, 95 (2016).
[15] Z. Konôpková, R. S. McWilliams, N. Gómez-Pérez, and A. F. Goncharov, Nature (London) **534**, 99 (2016).
[16] C. T. Seagle, E. Cottrell, Y. Fei, D. R. Hummer, and V. B. Prakapenka, Geophys. Res. Lett. **40**, 5377 (2013).
[17] S. Suehiro, T. Wakamatsu, K. Ohta, K. Hirose, and Y. Ohishi, High Press. Res. **39**, 579 (2019).
[18] See Supplemental Material at http://link.aps.org/supplemental/10.1103/PhysRevLett.125.078501 for detailed electrical resistivity measurements in hcp Fe at high pressure-temperature, texture effects of hcp Fe, first-principles molecular dynamics computations, estimations for the adiabatic heat flow and the energy balance of the core.
[19] G. Matassov, Ph.D. thesis, University of California, 1977.
[20] J. Xu, P. Zhang, K. Haule, J. Minar, S. Wimmer, H. Ebert, and R. E. Cohen, Phys. Rev. Lett. **121**, 096601 (2018).
[21] H. Gomi, K. Hirose, H. Akai, and Y. Fei, Earth Planet. Sci. Lett. **451**, 51 (2016).
[22] H. Gomi and K. Hirose, Phys. Earth Planet. Inter. **247**, 2 (2015).
[23] M. Pozzo, C. Davies, D. Gubbins, and D. Alfè, Phys. Rev. B **87**, 014110 (2013).
[24] M. Pozzo, C. Davies, D. Gubbins, and D. Alfè, Earth Planet. Sci. Lett. **393**, 159 (2014).
[25] L. Deng, C. Seagle, Y. Fei, and A. Shahar, Geophys. Res. Lett. **40**, 33 (2013).
[26] W. Yong, R. A. Secco, J. A. H. Littleton, and R. E. Silber, Geophys. Res. Lett. **46**, 11065 (2019).
[27] Q. Williams, Annu. Rev. Earth Planet Sci. **46**, 47 (2018).
[28] A. Hasegawa, T. Yagi, and K. Ohta, Rev. Sci. Instrum. **90**, 074901 (2019).
[29] Z. Konôpková, P. Lazor, A. F. Goncharov, and V. V. Struzhkin, High Press. Res. **31**, 228 (2011).
[30] D. Dobson, Nature (London) **534**, 45 (2016).
[31] C. Q. Choi, Proc. Natl. Acad. Sci. U.S.A. **114**, 1215 (2017).
[32] L. Pourovskii, J. Mravlje, A. Georges, S. Simak, and I. Abrikosov, New J. Phys. **19**, 073022 (2017).
[33] V. Drchal, J. Kudrnovský, D. Wagenknecht, I. Turek, and S. Khmelevskyi, Phys. Rev. B **96**, 024432 (2017).
[34] H. Inoue, S. Suehiro, K. Ohta, K. Hirose, and Y. Ohishi, Earth Planet. Sci. Lett. **543**, 116357 (2020).
[35] J. Wicht and S. Sanchez, Geophys. Astrophys. Fluid Dyn. **113**, 2 (2019).
[36] P. E. Driscoll and Z. Du, Geophys. Res. Lett. **46**, 7982 (2019).
[37] M. G. Buehler and W. R. Thurber, J. Electrochem. Soc. **125**, 645 (1978).
[38] V. Prakapenka, A. Kubo, A. Kuznetsov, A. Laskin, O. Shkurikhin, P. Dera, M. Rivers, and S. Sutton, High Press. Res. **28**, 225 (2008).
[39] C. Zhang, J.-F. Lin, Y. Liu, S. Feng, C. Jin, M. Hou, and T. Yoshino, J. Geophys. Res. **123**, 3564 (2018).
[40] J. M. David and M. G. Buehler, Solid-State Electron. **20**, 539 (1977).
[41] Y. Fei, C. Murphy, Y. Shibazaki, A. Shahar, and H. Huang, Geophys. Res. Lett. **43**, 6837 (2016).
[42] A. Dewaele, P. Loubeyre, F. Occelli, M. Mezouar, P. I. Dorogokupets, and M. Torrent, Phys. Rev. Lett. **97**, 215504 (2006).
[43] P. Giannozzi, S. Baroni, N. Bonini, M. Calandra, R. Car, C. Cavazzoni, D. Ceresoli, G. L. Chiarotti, M. Cococcioni, and I. Dabo, J. Phys. Condens. Matter **21**, 395502 (2009).
[44] K. F. Garrity, J. W. Bennett, K. M. Rabe, and D. Vanderbilt, Comput. Mater. Sci. **81**, 446 (2014).
[45] P. Allen, Phys. Rev. B **17**, 3725 (1978).
[46] A. Georges, G. Kotliar, W. Krauth, and M. J. Rozenberg, Rev. Mod. Phys. **68**, 13 (1996).
[47] G. Kotliar, S. Y. Savrasov, K. Haule, V. S. Oudovenko, O. Parcollet, and C. A. Marianetti, Rev. Mod. Phys. **78**, 865 (2006).
[48] M. Gurvitch, Phys. Rev. B **24**, 7404 (1981).
[49] P. B. Allen and B. Chakraborty, Phys. Rev. B **23**, 4815 (1981).
[50] P. B. Allen, in *Superconductivity in d- and f-Band Metals*, edited by H. Suhl, M. B. Maple (Elsevier, New York, 1980), pp. 291.
[51] M. Calandra and O. Gunnarsson, Phys. Rev. B **66**, 205105 (2002).
[52] O. Gunnarsson, M. Calandra, and J. Han, Rev. Mod. Phys. **75**, 1085 (2003).
[53] F. Rizzo, E. Cappelluti, and L. Pietronero, Phys. Rev. B **72**, 155113 (2005).
[54] K. Takenaka, J. Nohara, R. Shiozaki, and S. Sugai, Phys. Rev. B **68**, 134501 (2003).
[55] E. Yamasue, M. Susa, H. Fukuyama, and K. Nagata, Int. J. Thermophys. **24**, 713 (2003).
[56] K. Vafayi, M. Calandra, and O. Gunnarsson, Phys. Rev. B **74**, 235116 (2006).
[57] R. A. Secco, Phys. Earth Planet. Inter. **265**, 23 (2017).
[58] K. Ohta, Y. Nishihara, Y. Satoh, K. Hirose, T. Yagi, S. I. Kawaguchi, N. Hirao, and Y. Ohishi, Front. Earth Sci. **6**, 176 (2018).
[59] J.-F. Lin, Z. Mao, H. Yavaş, J. Zhao, and L. Dubrovinsky, Earth Planet. Sci. Lett. **298**, 361 (2010).
[60] H. K. Mao, J. Shu, G. Shen, R. J. Hemley, B. Li, and A. K. Singh, Nature (London) **396**, 741 (1998).
[61] H.-R. Wenk, S. Matthies, R. Hemley, H.-K. Mao, and J. Shu, Nature (London) **405**, 1044 (2000).
[62] S. Anzellini, A. Dewaele, M. Mezouar, P. Loubeyre, and G. Morard, Science **340**, 464 (2013).
[63] R. E. Silber, R. A. Secco, W. Yong, and J. A. Littleton, Sci. Rep. **8**, 10758 (2018).
[64] A. Pommier, Earth Planet. Sci. Lett. **496**, 37 (2018).
[65] J. Li and Y. Fei, in *Treatise on Geochemistry*, edited by K. K. Turekian (Elsevier, Oxford, 2014), pp. 527.
[66] K. Hirose, S. Labrosse, and J. Hernlund, Annu. Rev. Earth Planet Sci. **41**, 657 (2013).
[67] Y. Zhang, T. Sekine, H. He, Y. Yu, F. Liu, and M. Zhang, Sci. Rep. **6**, 22473 (2016).
[68] S. Suehiro, K. Ohta, K. Hirose, G. Morard, and Y. Ohishi, Geophys. Res. Lett. **44**, 8254 (2017).

[69] Y. Zhang, T. Sekine, J.-F. Lin, H. He, F. Liu, M. Zhang, T. Sato, W. Zhu, and Y. Yu, J. Geophys. Res. **123**, 1314 (2018).
[70] F. Nimmo, in *Treatise on Geophysics*, edited by G. Schubert (Elsevier, Oxford, 2015), pp. 27.
[71] A. M. Dziewonski and D. L. Anderson, Phys. Earth Planet. Inter. **25**, 297 (1981).
[72] G. M. Manthilake, N. de Koker, D. J. Frost, and C. A. Mccammon, Proc. Natl. Acad. Sci. U.S.A. **108**, 17901 (2011).
[73] V. Haigis, M. Salanne, and S. Jahn, Earth Planet. Sci. Lett. **355–356**, 102 (2012).
[74] B. Wu, P. Driscoll, and P. Olson, J. Geophys. Res. **116** (2011).
[75] K. Ohta, T. Yagi, N. Taketoshi, K. Hirose, T. Komabayashi, T. Baba, Y. Ohishi, and J. Hernlund, Earth Planet. Sci. Lett. **349–350**, 109 (2012).
[76] W.-P. Hsieh, F. Deschamps, T. Okuchi, and J.-F. Lin, Proc. Natl. Acad. Sci. U.S.A. **115**, 4099 (2018).
[77] W.-P. Hsieh, F. Deschamps, T. Okuchi, and J.-F. Lin, J. Geophys. Res. **122**, 4900 (2017).
[78] F. Deschamps and W.-P. Hsieh, Geophys. J. Int. **219**, S115 (2019).
[79] K. Ohta, T. Yagi, K. Hirose, and Y. Ohishi, Earth Planet. Sci. Lett. **465**, 29 (2017).
[80] B. A. Buffett, H. E. Huppert, J. R. Lister, and A. W. Woods, Nature (London) **356**, 329 (1992).
[81] A. Corgne, S. Keshav, Y. Fei, and W. F. McDonough, Earth Planet. Sci. Lett. **256**, 567 (2007).
[82] P. Olson, Science **342**, 431 (2013).
[83] A. J. Biggin, E. J. Piispa, L. J. Pesonen, R. Holme, G. A. Paterson, T. Veikkolainen, and L. Tauxe, Nature (London) **526**, 245 (2015).
[84] R. K. Bono, J. A. Tarduno, F. Nimmo, and R. D. Cottrell, Nat. Geosci. **12**, 143 (2019).